

# *In situ* interferometric alignment systems for the assembly of microchannel relay systems

Brian Robertson, Yongsheng Liu, Guillaume C. Boisset, Mohammad R. Tagizadeh, and David V. Plant

An interferometric alignment technique developed for the assembly of microchannel relay systems is described. The method uses pairs of diffractive lenslets that are arranged to form compact *in situ* interferometers. The relative transverse, longitudinal, and rotational alignment of the two lenslet arrays can be quantitatively determined from the resulting interference patterns. The theoretical analysis is compared with the experimental performance. © 1997 Optical Society of America

*Key words:* Alignment, interferometric, lenslet array packaging.

## 1. Introduction

One of the key problems affecting the implementation of practical free-space microchannel relay systems is that of alignment. Several methods for prealigning lenslet arrays with respect to optoelectronic-device arrays based on the imaging of fiducial alignment marks,<sup>1</sup> Moiré patterns,<sup>2</sup> or flip chip bonding<sup>3</sup> have been demonstrated. These techniques are typically employed when the two alignment planes are close together. When the two planes are separated by several millimeters, active alignment or Fresnel zone plates fabricated on the device arrays<sup>4</sup> can be used to aid alignment. Here an interferometric alignment technique developed for the assembly and manufacture of microchannel relay systems is described. The approach uses *in situ* interferometers formed from pairs of low-efficiency diffractive lenslets. The resulting interference patterns can be used to calculate the relative alignment of two relatively widely separated lenslet arrays. We present a theoretical analysis of this technique and describe the performance of a prototype interferometric alignment system developed for use within a free-space photonic back plane.

## 2. Description of Alignment Technique

The operation of the interferometric alignment system is described in Fig. 1. Additional interferometric alignment lenses  $L_{A1}$  and  $L_{A2}$  are fabricated around the edge of the signal lenslet arrays. Collimated light incident on the first interferometric alignment lenslet,  $L_{A1}$ , is diffracted into a series of wave fronts as shown in Fig. 2. For the purposes of this analysis the light diffracted into the  $m$ th diffraction order by lenslet  $L_{A1}$  is represented by the term  $L(A1, m)$ . In addition, we assume that only the undiffracted zeroth order,  $L(A1, 0)$ , and the +1 diffraction order,  $L(A1, +1)$ , are of interest. This assumption is based on the fact that only a small amount of the light diffracted into the other orders [ $L(A1, -1)$ ,  $L(A1, +2)$ ,  $L(A1, -2)$ , etc.] reaches the second lens facet owing to the high divergence of these beams when compared with the  $m = 0$  and  $m = +1$  diffraction orders. The generation of interference fringes by two parallel zone plates was described by Chau,<sup>5</sup> Koronkevich and Lenkova,<sup>6</sup> and Stevens.<sup>7</sup>

When the  $m = 0$  and  $m = +1$  wave fronts are incident on the second lenslet,  $L_{A2}$ , they generate a series of overlapping diffracted orders as shown in Fig. 2. For this analysis only the zeroth diffraction order (interference between the undiffracted light in wave front  $L(A1, 0)$  and the light originally in the  $L(A1, +1)$  order, which is diffracted by  $L_{A2}$  back into the zeroth order) are considered. At the second lenslet plane the various beams overlap to produce a complex interference pattern; however, the effect of the higher orders lessens as the light propagates away from the second lenslet array because of the divergence of these wave fronts.

B. Robertson, Y. Liu, G. C. Boisset, and D. V. Plant are with the Department of Electrical Engineering, McGill University, 3480 University Street, Montreal, Québec, Canada H3A 2A7. M. R. Tagizadeh is with the Department of Physics, Heriot-Watt University, Edinburgh EH14 4AS, Scotland, UK.

Received 9 April 1997; revised manuscript received 30 July 1997.  
0003-6935/97/359253-08\$10.00/0

© 1997 Optical Society of America

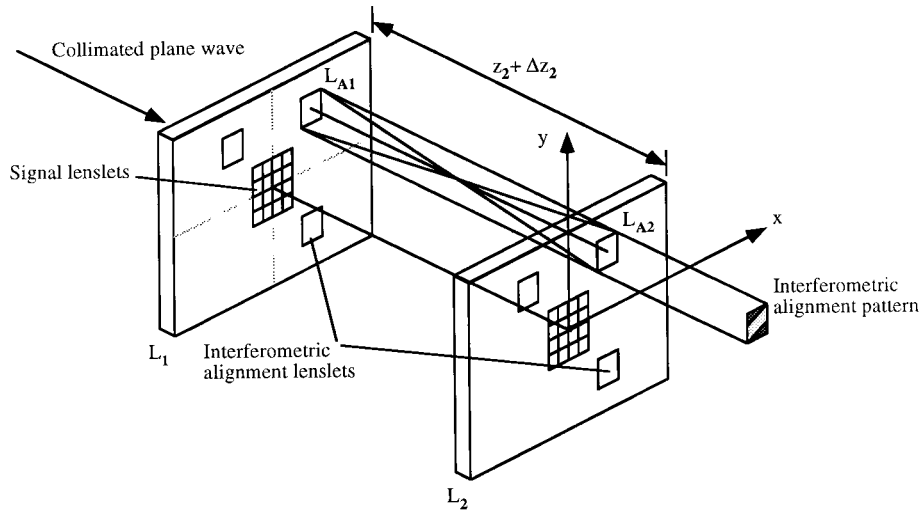


Fig. 1. Schematic outline of lenslet array alignment with *in situ* interferometers.

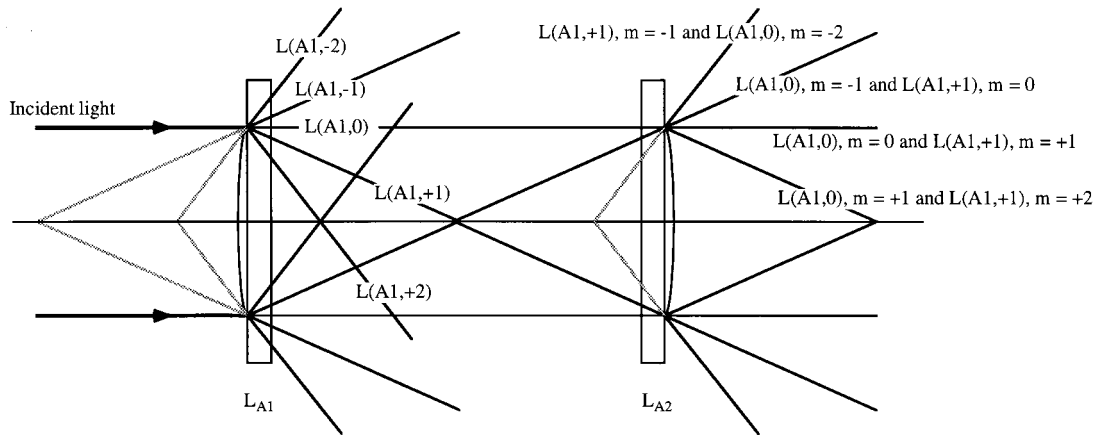


Fig. 2. Incident light diffracted by  $L_{A1}$  into  $m = +2, +1, 0, -1, -2$  orders and subsequent diffraction of  $L(A1, 0)$  and  $L(A1, +1)$  orders at lenslet  $L_{A2}$ . These beams overlap and produce an interference pattern dependent on the degree of misalignment between the lenslets.

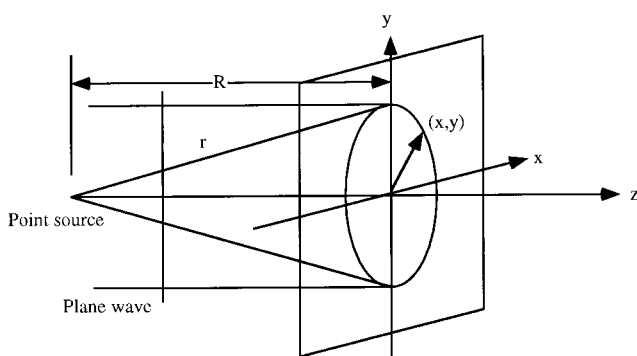


Fig. 3. Interference of plane wave and point source.

The term  $f_A$  represents the focal length of the alignment lenslets, where  $2f_A = z_2$ , the ideal separation between the two lenslet arrays. For a misalignment of  $\Delta z_2$  the light from the first lens facet in the  $L(A1, +1)$  order is a distance  $u = f_A + \Delta z_2$  from the second lens facet. Thus, after passing through the second

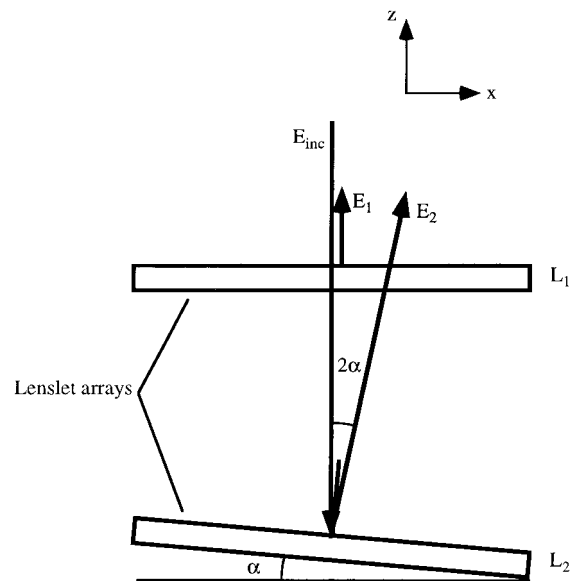
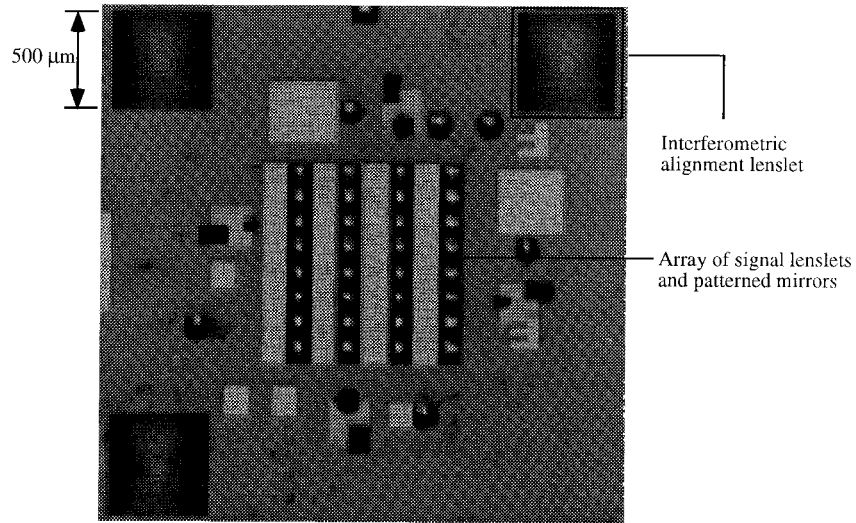
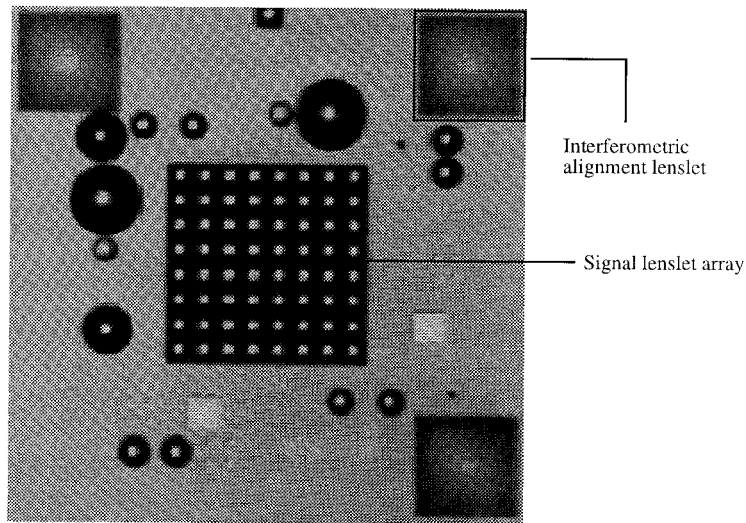


Fig. 4. Interference pattern caused by tilt of lenslet array  $L_2$  with respect to lenslet array  $L_1$ .



(a)



(b)

Fig. 5. Photographs of the two lenslet arrays, (a)  $L_1$  and (b)  $L_2$ , used in the experiment.

lens facet, this light appears to come from a point that is a distance  $v$  from  $L_{A2}$ , where

$$1/v = 1/f_A - 1/u. \quad (1)$$

The field that is due to a point source a distance  $R$  away from the source and at a point  $(x, y)$  normal to the optical axis is given by

$$u_1 = (A/r)\exp[i(kr - \omega t)]. \quad (2)$$

This geometry is illustrated in Fig. 3.  $A$  is a complex constant dependent on the field strength,  $R = v$ , and  $r$  is the distance from the point source to point  $(x, y)$  on the lens facet. Thus

$$r^2 = R^2 + x^2 + y^2. \quad (3)$$

Similarly, the field that is due to a plane wave can be written as

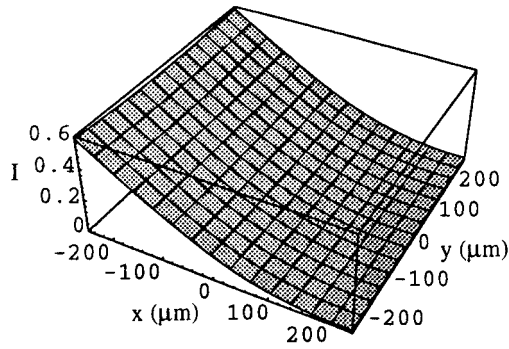
$$u_2 = B \exp[i(kR - \omega t + \psi)], \quad (4)$$

where  $B$  is a complex constant dependent on the field strength and  $\psi$  is a phase term. As both waves were derived from the same incident beam, there exists a certain initial phase relationship between them. The total field is therefore given by  $u_T = u_1 + u_2$ ,

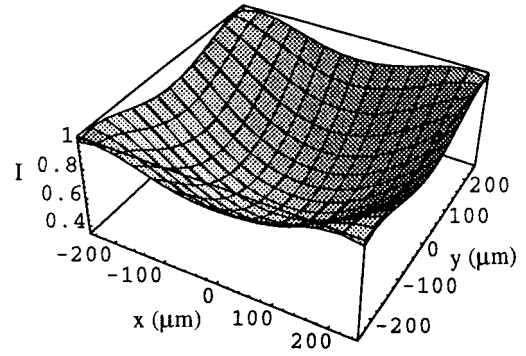
$$u_T = \{(A/r)\exp(ikr) + B \exp[i(kR + \psi)]\}\exp(i\omega t), \quad (5)$$

from which it follows that

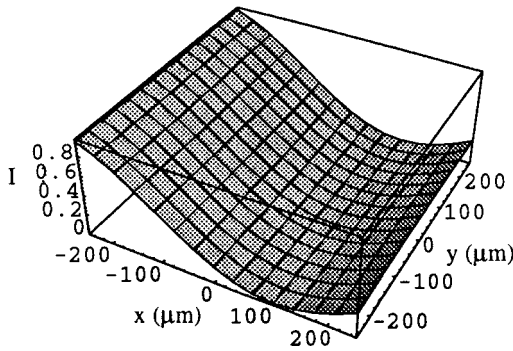
$$u_T = \{A/(R^2 + x^2 + y^2)^{1/2} \exp[ik(R^2 + x^2 + y^2)^{1/2}] + B \exp[i(kR + \psi)]\}\exp(i\omega t). \quad (6)$$



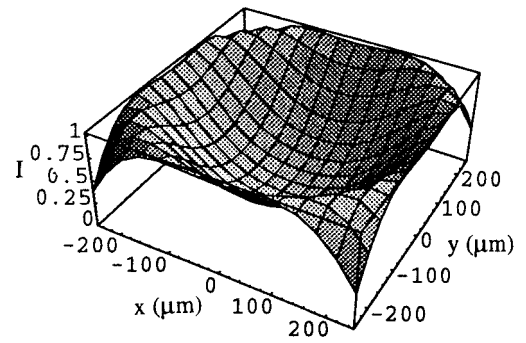
(a)



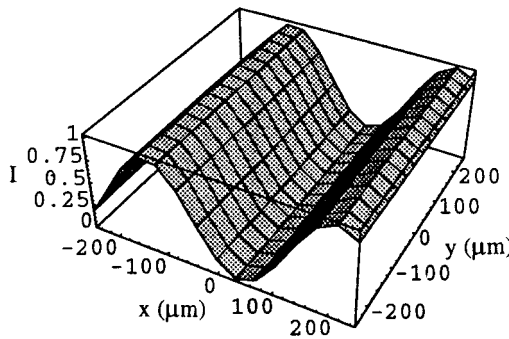
(a)



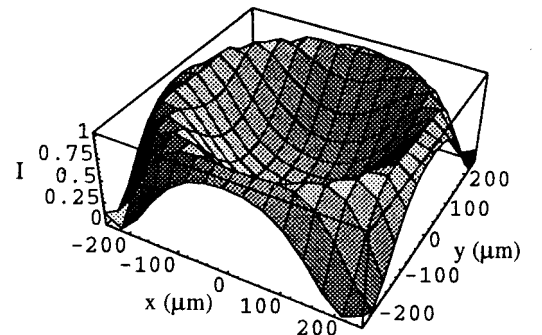
(b)



(b)



(c)



(c)

Fig. 6. Theoretical interference pattern for a misalignment of  $\Delta z = 0 \mu\text{m}$  and (a)  $\Delta x = 1 \mu\text{m}$ , (b)  $\Delta x = 2 \mu\text{m}$ , (c)  $\Delta x = 5 \mu\text{m}$ .

Fig. 7. Theoretical interference pattern for a misalignment of  $\Delta x = 0 \mu\text{m}$  and (a)  $\Delta z = 25 \mu\text{m}$ , (b)  $\Delta z = 50 \mu\text{m}$ , (c)  $\Delta z = 75 \mu\text{m}$ .

The resulting irradiance at point  $I(x, y)$  can therefore be determined as

$$I(x, y) = (|A|/r)^2 + |B|^2 + [2|A||B|/(R^2 + x^2 + y^2)^{1/2}] \times \cos[k(R^2 + x^2 + y^2)^{1/2} + \psi]. \quad (7)$$

If the lenslets are translated a distance  $\Delta x$  with respect to each other,  $L(A1, +1)$  is diffracted by  $L_{A2}$  at an angle  $\beta$  to the optic axis, where

$$\tan \beta = (\Delta x/f_A). \quad (8)$$

For small translational misalignments the field  $u_1$  can be written as

$$u_1 = A/r \exp[i(kr - \omega t)] \exp[ikx \sin \beta] \quad (9)$$

(i.e., we are simply adding a linear phase shift). This is valid if there is no longitudinal misalignment ( $\Delta z_2 = 0$ ). Thus the number of fringes,  $N$ , observed across a lenslet interferometer of dimensions  $D_L \times D_L$  will be given by

$$N = (D_L \sin \beta)/\lambda. \quad (10)$$

**Table 1. Number of Fringes Observed,  $N$ , for a Given Translational Misalignment  $\Delta x$  and Relative Misalignment  $\Delta x/D_L$**

$\Delta x$ ( $\mu\text{m}$ )	$\beta$	$N$	$\Delta x/D_L$
1	0.021	0.3	0.002
2	0.042	0.6	0.004
3	0.064	0.9	0.006
4	0.085	1.2	0.008
5	0.106	1.5	0.010
6	0.127	1.8	0.012
7	0.149	2.0	0.014
8	0.169	2.3	0.016
9	0.191	2.6	0.018
10	0.212	2.9	0.020

In the case of a pure longitudinal misalignment the number of circular fringes observed,  $m$ , is given by

$$m = \{[v^2 + (D_L/2)^2]^{1/2} - v\}/\lambda, \quad (11)$$

where

$$v = f_A(f_A + \Delta z_2)/\Delta z_2. \quad (12)$$

The effect of a simultaneous longitudinal and translational misalignment is the formation of decentered circular fringes.

### 3. Interferometric Tilt Alignment

Interferometric alignment techniques can also be used to minimize the tilt angle between two different lenslet arrays or between an optoelectronic-device array and a lenslet array. We assume that the tilt angle is small enough to ensure that scalar theory holds. Figure 4 shows the basic approach used to align two lenslet arrays. A plane wave front  $E_{\text{inc}}$  is normally incident on  $L_1$ . A fraction of the light is reflected by both  $L_1$  and  $L_2$  (pixelated antireflective coatings or thin partial reflecting mirrors can be in-

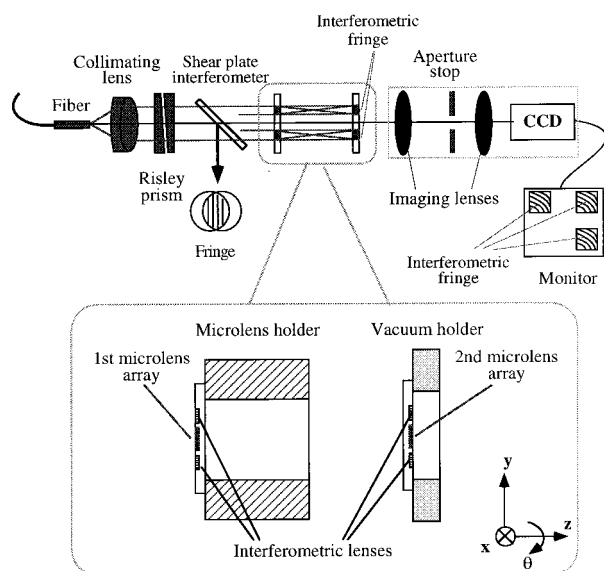


**Fig. 8. Diagram of optical system used to align the two lenslet arrays.**

tegrated with the lenslets for this purpose). If lenslet array  $L_2$  is tilted at an angle of  $\alpha$  with respect to  $L_1$ , a series of periodic plane interference fringes is observed. The period of the fringes,  $T$ , will be determined by the relative tilt angle, and the contrast ratio will be governed by the relative reflectivity of the two lenslet arrays. The two reflected wave fronts  $E_1$  and  $E_2$  are shown in Fig. 4, where  $E_1 = E_{01} \exp\{i[\mathbf{k}_1(\mathbf{r} - wt)]\}$  and  $E_2 = E_{02} \exp\{i[\mathbf{k}_2(\mathbf{r} - wt + \phi)]\}$ . It is assumed that the propagation vectors lie in the  $x$ - $z$  plane; thus  $\mathbf{k}_1 = (0, 0, k)$ ,  $\mathbf{k}_2 = (k \sin 2\alpha, 0, k \cos 2\alpha)$ , and  $k = 2\pi/\lambda$ . In addition, the incident electric field is taken to be parallel to the  $x$  axis. As long as the tilt angle is small (order of a degree or so), we need not be concerned with vector effects; thus the irradiance  $I_T(x, z)$  is given by

$$I_T(x, y) = I_1 + I_2 + 2\sqrt{I_1 I_2} \times \cos(kx \sin 2\alpha + kz \cos 2\alpha + \phi), \quad (13)$$

where  $I_1 = |E_{01}|^2$  and  $I_2 = |E_{02}|^2$ . Thus the period of the interference fringes,  $T$ , in the  $x$  direction (what is measured experimentally) is given by

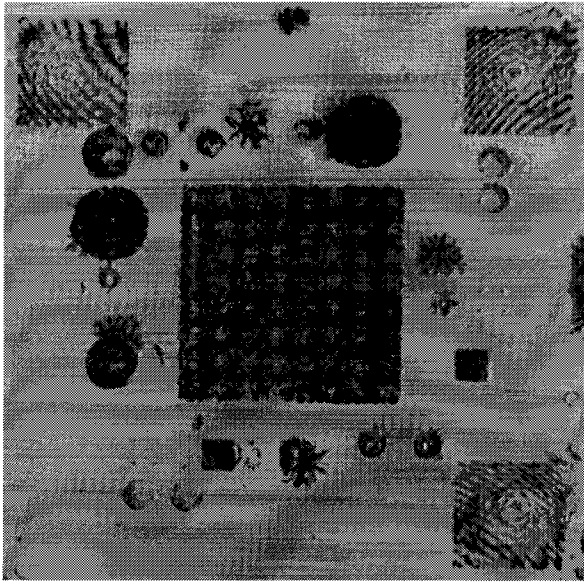
$$T = \lambda/\sin 2\alpha. \quad (14)$$

Thus a tilt misalignment of greater than  $\pm 0.01^\circ$  requires a fringe period of  $T > 1.813$  mm at 632.8 nm.

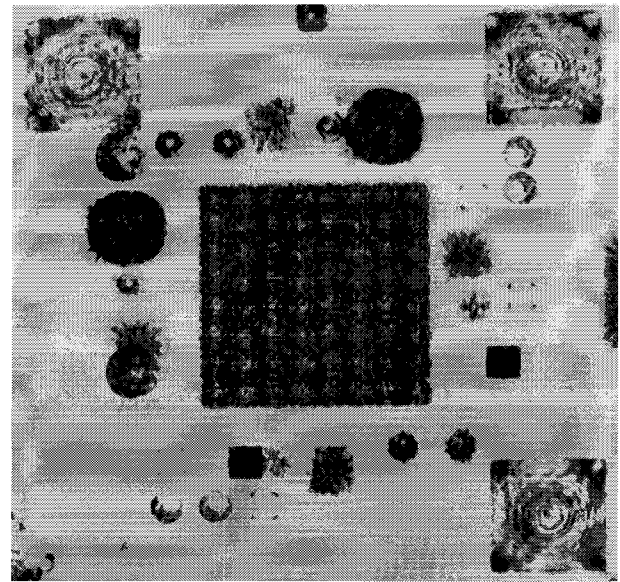
### 4. Test Element Design

To verify the practicality of this technique, we incorporated a set of interferometric alignment elements within a microchannel relay (Fig. 1). The microchannel interconnect formed part of a hybrid relay system intended for use within a prototype free-space photonic back plane.<sup>8</sup> Figures 5(a) and 5(b) show photographs of the two diffractive optical elements used in this experiment. The interconnection lenslets were designed to have a focal length  $f_i$  of 768  $\mu\text{m}$  at a wavelength of  $\lambda = 850$  nm and dimensions of 125  $\mu\text{m} \times 125$   $\mu\text{m}$ , and were fabricated with eight phase levels. The interconnect employed a maximum lens-to-waist geometry,<sup>9</sup> where  $z_2 = 2(f_i + f_i^2/2z_R)$ ,  $z_R = \pi w_0^2/\lambda$ , and  $w_0$  is the input beam radius, set at 12.5  $\mu\text{m}$ . These parameters resulted in a lenslet-to-lenslet spacing (optical distance) of 5.40 mm.

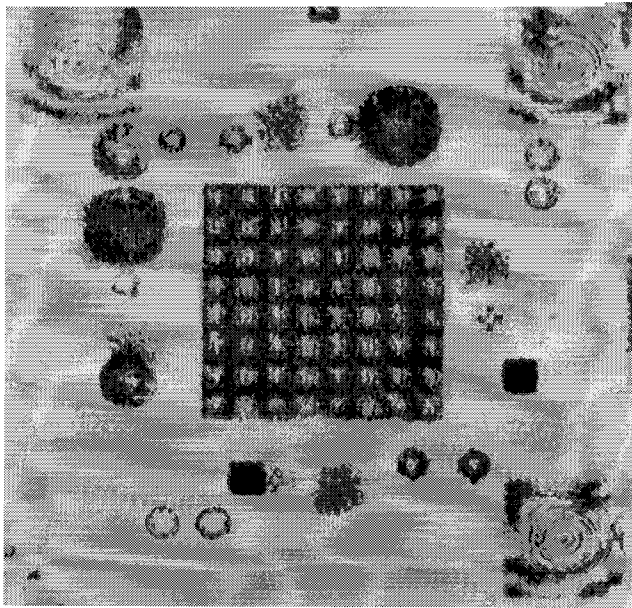
Three sets of diffractive alignment lenslets were fabricated around the edge of the interconnection elements as shown in Fig. 5. These components had dimensions of 500  $\mu\text{m} \times 500$   $\mu\text{m}$  and a focal length  $f_A$  of  $z_2/2 = 2.70$  mm at an operating wavelength of 632.8 nm. For the contrast of the resulting interference fringes to be maximized, approximately equal amounts of power must be diffracted into the zeroth and +1 diffraction orders. To achieve this, we fabricated the alignment lenses as binary elements with a  $\pi$  phase delay at 850 nm. Thus by using straightforward scalar diffraction theory we can show that the power in the zeroth,  $P_0$ , and +1 diffraction orders,



(a)



(c)



(b)

Fig. 9. Photographs of fringe patterns obtained during alignment. (a) Severe rotational misalignment and misalignment in the  $x$ ,  $y$ , and  $z$  directions. (b) Rotational misalignment corrected and misalignment in the  $y$  direction dominant. (c) Final alignment.

$P_0$  and  $P_{+1}$ , equals

$$P_0 = P_{\text{inc}}/2(1 + \cos k\pi), \quad (15)$$

$$P_{+1} = (2P_{\text{inc}}/\pi^2)(1 - \cos k\pi), \quad (16)$$

where

$$k = (\lambda_e/\lambda_0)[n_s(\lambda_0) - 1]/[n_s(\lambda_e) - 1]. \quad (17)$$

The term  $P_{\text{inc}}$  represents the incident power,  $\lambda_e$  is the wavelength for which the interferometric alignment lens has been etched,  $\lambda_0$  is the illumination wavelength, and  $n_s(\lambda)$  is the refractive index of the substrate at wavelength  $\lambda$ . Thus in the case of a fused-silica

substrate, where  $\lambda_e = 850$  nm and  $\lambda_0 = 632.8$  nm, it follows that  $P_0 = 0.282P_{\text{inc}}$  and  $P_{+1} = 0.291P_{\text{inc}}$ . Thus an approximately equal amount of incident light ends up in both the zeroth and the +1 diffraction orders. Measurements on the interferometric alignment lens showed that  $P_0 = 0.29P_{\text{inc}}$  and  $P_{+1} = 0.24P_{\text{inc}}$ , close to the theoretically predicted values.

From Eq. 7, the theoretical interference pattern was calculated for the parameters  $f_A = 2.70$  and  $\lambda = 632.8$  nm. For simplicity, the power in the two wave fronts was taken to be exactly equal and  $\psi = 0$ . The theoretical interference pattern is shown in Fig. 6 for a misalignment of  $\Delta z = 0$   $\mu\text{m}$  and  $\Delta x = 1, 2, 5$   $\mu\text{m}$ ,

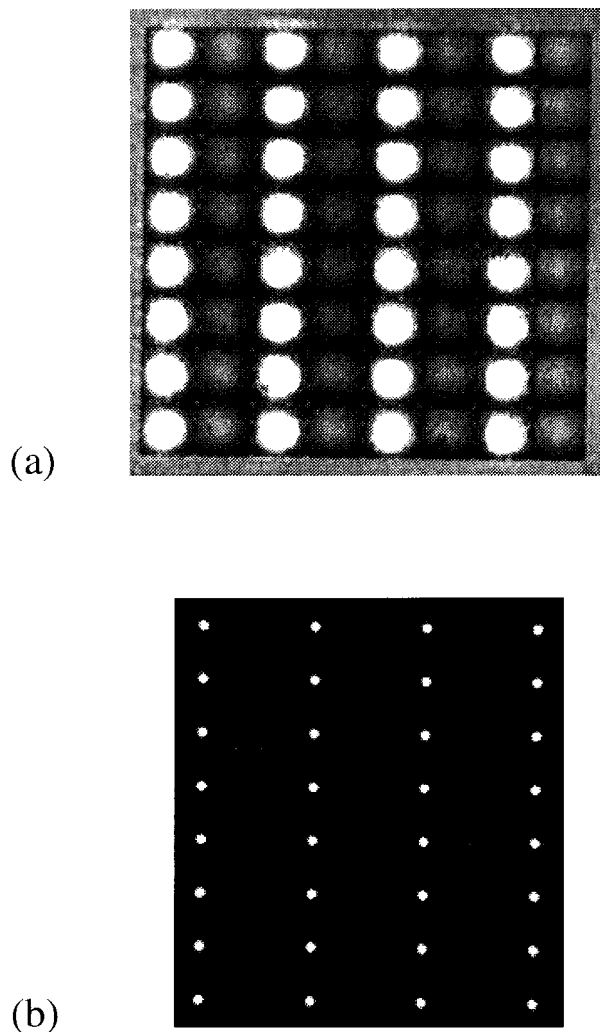


Fig. 10. Performance of aligned lenslet arrays: (a)  $4 \times 8$  array of beams relayed through the interconnect at the second lenslet array and (b) focused beams at the output focal plane.

and in Fig. 7 for  $\Delta x = 0 \mu\text{m}$  and  $\Delta z = 25, 50, 75 \mu\text{m}$ . From these results it can be seen that even small translational misalignments of the order of a micrometer produce visible fringes. However, longitudinal misalignments of the order of  $50 \mu\text{m}$  are required before an equally discernible fringe pattern can be observed. Table 1 lists the number of fringes observed across the experimental *in situ* interferometer aperture for a given translational misalignment with zero longitudinal misalignment. In addition, the relative misalignment  $\Delta x/D_L$  is given.

### 5. Alignment System

The two lenslet arrays were mounted on opposite sides of the cylindrical component holder shown in Fig. 8. The first stage of assembly involved mounting a polarizing beam splitter and quarter-wave-plate assembly within the holder. We then positioned the first lenslet array with respect to the cylinder by using chrome alignment markers, and we glued it in place. Figure

8 shows the system used to align the lenslet arrays with respect to each other. Light from an He-Ne laser was launched into a single-mode fiber, and the output from the fiber was then collimated by use of a single achromat. The collimation of the illumination beam was tested with a commercial shear plate interferometer.<sup>10</sup> A Risley beam steerer, consisting of a pair of wedged prisms, was adjusted to ensure that the He-Ne beam was incident normal to the surface of the first microlens array. The lenslet array component holder could be translated in the  $x$ - $y$  direction (normal to the beam) and rotated about the beam axis. The second microlens array was attached to a vacuum holder that could be moved in the  $z$  direction (parallel to the beam). Using a vacuum holder to mount the lenslet has several advantages, including simplicity of design and the ease with which it can be detached from the microlens array. The whole system was constructed with a Spindler & Hoyer microbench set.

When the second microlens array was brought into position, a series of interferometric fringes was formed as described in Section 2. The fringes were imaged onto a CCD camera for further processing and analysis. For the contrast of these fringes to be enhanced, an aperture stop was placed in the optical path of the imaging system to block stray light from reaching the CCD. This also partially blocked some of the higher-order diffracted beams, which also enhanced the fringe contrast ratio.

### 6. Experimental Results

Figure 9 shows the interference fringes observed as the second lenslet array was brought into alignment with the first. Figure 9(a) illustrates the fringe pattern for the case in which the two lenslets were severely rotationally misaligned in  $\theta$  and misaligned in the  $x$ ,  $y$ , and  $z$  directions. When the second microlens array was moved closer to its nominal position, the number of fringes observed was reduced. Figure 9(b) shows the fringe pattern for the situation in which the rotational misalignment was corrected and misalignment in the  $y$  direction was dominant. Final alignment was obtained when the number of fringes was minimized as shown in Fig. 9(c). Note that in this experiment the dimensions of the microlens holder were slightly larger than the design value owing to an increase in dimensions that occurred during anodization. In addition, the separation between lenslets was slightly larger owing to the thickness of glue used [Dow Corning 732 room temperature vulcanizing (RTV) sealant, estimated to be  $100$ – $150 \mu\text{m}$  thick]. The optical distance between the two lenslets was measured with a traveling microscope and found to be  $5.60 \text{ mm}$ . The final fringe patterns observed resemble closely the theoretically predicted irradiance distributions shown in Figs. 6 and 7.

When the two microlens arrays were optimally aligned, the second microlens was glued to the component holder. However, when the assembled unit was detached from the alignment system, a translational misalignment in the  $x$  direction of approximately one fringe ( $\sim 3 \mu\text{m}$ ) occurred. This is

believed to be due to the stress introduced by the alignment rig during assembly.

To test the finally aligned module, we relayed a  $4 \times 8$  array of spots with a pitch of  $125 \mu\text{m}$  in the vertical direction and  $250 \mu\text{m}$  in the horizontal direction through the microlens arrays. Figure 10 shows the resulting spot pattern produced by the beams after the second microlens array. From this result it can be seen that there was little rotational misalignment between the two lenslet arrays. The slight error that did occur happened during the gluing stage and was again attributed to stress introduced by the Spindler & Hoyer alignment rig. The overall performance of this technique would be improved by use of a more stable alignment system.

## 7. Conclusions

We have presented a novel technique for quantitatively aligning microlens arrays by use of compact *in situ* interferometers based on pairs of low-efficiency diffractive lenslets. The interference patterns are formed by the interaction of the zeroth and +1 diffraction orders of the lenslets. For the powers in these two beams to be balanced, the lenslets are designed for operation at  $632.8 \text{ nm}$  and etched for  $850 \text{ nm}$ . This allows an approximately equal amount of light to be present in both orders when the interferometers are illuminated at  $632.8 \text{ nm}$ . The relative transverse, longitudinal, and rotational alignment of the lenslet arrays can be determined from the resulting interference patterns. The initial set of experimental results presented here illustrates that this technique can be used to obtain transverse alignment of device planes of the order of  $\pm 1 \mu\text{m}$  and longitudinal alignment information to within  $\pm 50 \mu\text{m}$ . In addition, by using multiple interferometers one can achieve accurate rotational alignment of device planes. Alignment of multiple optical layers with this technique requires separate interferometers for each successive stage.

Future research will include the development of a more rigorous model capable of determining the ef-

fect that higher diffraction orders have on the interference patterns. In addition, we intend to implement image-processing software designed to analyze the interference patterns and determine the relative misalignments of the lenslet arrays.

D. V. Plant acknowledges support from the Canadian Institute of Telecommunications Research. This research was also supported by the Nortel/National Science and Engineering Research Council Chair in Photonics Systems.

## References

1. J. M. Sasian and D. A. Baillie, "Simple technique for out-of-focus feature alignment," *Opt. Eng.* **34**, 564–566 (1995).
2. S. K. Patra, J. Ma, V. H. Ozguz, and S. H. Lee, "Alignment issues in packaging for free-space optical interconnects," *Opt. Eng.* **33**, 1561–1570 (1994).
3. Y. C. Lee and N. Basavanthally, "Solder engineering for optoelectronic packaging," *J. Metals* **46**, 46–50 (1994).
4. G. C. Boisset, B. Robertson, W. S. Hsiao, M. R. Taghizadeh, J. Simmons, K. Song, M. Matin, D. A. Thompson, and D. V. Plant, "On-die diffractive alignment structures for packaging of microlens arrays with 2-D optoelectronic device arrays," *IEEE Photon. Technol. Lett.* **8**, 918–920 (1996).
5. H. H. M. Chau, "Demonstration of white-light interference on two spaced parallel zone plates," *Appl. Opt.* **9**, 1722–1723 (1970).
6. V. P. Koronkevich and G. A. Lenkova, "Diffractive interferometer," *Avtometriya* **3**, 61–67 (1984) [*Autom. Monit. Meas.* **3**, (1984)].
7. R. F. Stevens, "Zone-plate interferometer," *J. Mod. Opt.* **35**, 75–79 (1988).
8. D. V. Plant, B. Robertson, H. S. Hinton, M. H. Ayliffe, G. C. Boisset, D. J. Goodwill, D. N. Kabal, R. Iyer, Y. S. Liu, D. R. Rolston, W. M. Robertson, and M. R. Taghizadeh, "A multi-stage CMOS-SEED optical backplane demonstration system," in *International Conference on Optical Computing 96*, Vol. 139 of Institute of Physics Conference Series (Institute of Physics, Bristol, UK, 1996), pp. 14–15.
9. F. B. McCormick, F. A. P. Tooley, T. J. Cloonan, J. M. Sasian, and H. S. Hinton, "Optical interconnections using microlens arrays," *Opt. Quantum Electron.* **24**, 5465–5477 (1992).
10. Technical catalog, section 64-12, 1995/1996 (Melles Griot, U.S.A.).